

Franck–Condon Simulations of Clusters: Phenol–Nitrogen

Igor Pugliesi,[†] M. J. Watkins, and Klaus Müller-Dethlefs*

York Centre of Laser Spectroscopy (YCLS), Department of Chemistry, The University of York, Heslington, York YO10 5DD, U.K.

Received: August 15, 2005

Multidimensional Franck–Condon simulations of the resonance enhanced multiphoton ionization (REMPI) and mass-analyzed threshold ionization (MATI) spectra of phenol–nitrogen are obtained from CASSCF, MRCI, and SACCI optimized geometries. In the REMPI simulations, the results are unsatisfactory, as the transitions associated with intermolecular modes are widely underestimated and much less intense than those associated with intramolecular modes. Conversely, the simulations of the MATI spectra show a good similarity to experiment. The best simulations are obtained in both instances from the SACCI optimized geometries. Furthermore, the simulations suggest that the two most prominent Franck–Condon envelopes present in the MATI spectra are due to the σ and $\sigma + n\gamma'$ combination bands in accord with the assignments of the MATI spectra of the analogous phenol–carbon monoxide cluster.

1. Introduction

Due to the prime importance of Franck–Condon integrals in spectroscopy and reaction dynamics,^{1–4} a variety of approaches have been developed for their evaluation. A major problem that prevents multidimensional Franck–Condon integrals from being reduced to simple products of one-dimensional integrals, resulting in their evaluation being complicated and computer intensive, is posed by the rotation and mixing of the normal modes of one electronic state in the normal-mode basis of the other electronic state involved in an electronic transition. This phenomenon was first considered by Duschinsky⁵ when extending the Franck–Condon principle from diatomics to polyatomic molecules. Duschinsky proposed that the two sets of normal coordinates are related to each other by a linear transformation. This so-called Duschinsky transformation cannot, however, be regarded as a general treatment, as the relationship between the normal coordinates of different electronic states of a polyatomic molecule is generally neither linear nor orthogonal. However, the linear/orthogonal transformation proposed by Duschinsky is widely accepted and is a useful tool in vibronic analysis.

Through the generating function formalism, Sharp and Rosenstock⁶ were the first to solve the Franck–Condon integral problem for polyatomic molecules including the Duschinsky effect. Their equations express individual Franck–Condon integrals by a finite series expansion. This approach was the first of its kind and provided a general basis for later methodologies. Amongst these, one of the most commonly used is the coherent state method developed by Doktorov et al.⁷ It yields the same expression as the method of Sharp and Rosenstock. The solution of a multidimensional Franck–Condon integral is now achieved by recurrence relations, which are exact in the harmonic approximation. A detailed derivation of these relations can be found in refs 7 and 10.

The coherent state method has been extensively applied to large polyatomic molecules. Guner et al.⁸ were the first to use

this method to simulate vibronic spectra of large molecules. Callis et al.⁹ applied the method to the fluorescence spectra of indole, and Berger et al.¹⁰ applied it to the simulation of sequence band spectra of benzene and pyrazine. Recently, multidimensional Franck–Condon simulations of the dispersed fluorescence (DF) spectra of phenol have been carried out by Schumm et al.¹¹ The S_0 and S_1 equilibrium geometries used in these simulations were obtained at the (8,7)-CASSCF/cc-pVDZ level of theory. These simulations reproduced the main spectral features, but the intensities of several vibronic transitions were either under- or overestimated. A much better agreement between simulation and experiment was obtained by manually altering the S_1 state CASSCF geometry (shortening the C–O bond and elongating along the coordinate of mode 6a). The structural corrections carried out by Schumm have further been corroborated by Spangenberg et al.,¹² who have developed a Franck–Condon fit program that alters the geometries of the states involved in the electronic transition until a best match between the simulated and experimental intensities is obtained.

Studies 11 and 12 indicate that vibronic transition intensities are extremely sensitive to the upper and lower state geometries and therefore that Franck–Condon simulations of vibronic spectra of polyatomic molecules can provide very accurate means to assess the quality of the calculated ab initio geometries. In our previous review, we generated Franck–Condon simulations with geometries obtained from the highly correlated post-Hartree–Fock methods MRCI and SACCI.¹³ While the simulations based on MRCI optimized geometries are very similar to the CASSCF simulations in ref 11 and fail to reproduce the experimentally measured intensities faithfully, the simulations obtained from SACCI optimized geometries are very close to the experimental spectra. It is interesting to extend the ideas and results from the above study to phenol clusters such as phenol–nitrogen, as the simulations of their resonance enhanced multiphoton ionization (REMPI) and zero electron kinetic energy (ZEKE)/mass-analyzed threshold ionization (MATI) spectra represent a more rigorous test for the electronic structure methods employed in ref 13.

Extensive experimental and theoretical analysis carried out by the group of Müller-Dethlefs^{14–16} has shown that, among

* Corresponding author. Present address: The Photon Science Institute, Simon Building, The University of Manchester, Manchester M13 9PL, U.K. E-mail: k.muller-dethlefs@manchester.ac.uk. Phone: +44 (0)161 275 1000.

[†] E-mail: igor.pugliesi@gmail.com.

the clusters formed between aromatic molecules and gases, phenol–nitrogen is unique in the structure it adopts. The binding between the two moieties is dominated by dipole–quadrupole interactions in the neutral ground and first excited states, and by charge–quadrupole interactions in the cationic ground state. This causes the nitrogen molecule to bind in-plane with the hydrogen of the OH group, rather than binding above the aromatic ring, as favored by van der Waals clusters such as phenol–argon. These findings were corroborated by an extensive *ab initio* CASSCF study of Watkins et al.,¹⁷ which showed this level of theory to give a good description of the intermolecular potential energy surface, reflected among other properties in a very good agreement between calculated and experimental frequencies of the intermolecular modes and rotational constants. Fuji et al.¹⁸ have investigated the phenol–nitrogen binding by IR–UV double resonance spectroscopy. They found that the red shift of the OH stretching frequency in the S_0 and S_1 states is considerably smaller compared to other hydrogen-bond-type phenol clusters such as phenol–water, corroborating the fact that the binding between the phenol and nitrogen moieties is a “hybrid” between a hydrogen bond and a van der Waals bond. The analysis of the cluster cation via IR spectroscopy confirmed that in the D_0 state the complex also adopts in-plane binding between the two moieties.¹⁹ A precise determination of the structural parameters of the S_0 and S_1 states was achieved by Schmitt et al. through fits to high resolution rotational laser induced fluorescence (LIF) spectra.²⁰

Phenol–nitrogen is a well characterized species and can therefore be used to further investigate the applications of multidimensional Franck–Condon simulations to a large system involving a mixture of covalent and noncovalent interactions. As the vibronic transition intensities associated with intermolecular modes of a cluster are even more sensitive to geometry changes than vibronic transitions of a monomer, Franck–Condon simulations of vibronic spectra of phenol–nitrogen are an even stricter test of the quality of the *ab initio* geometries obtained.

Franck–Condon simulations of the phenol–nitrogen ZEKE spectra along the intermolecular stretching mode σ have been previously carried out by Haines et al.¹⁴ They used single coordinate Morse potentials derived from experimental binding energies and spectroscopic constants. They showed that the σ progression observed in the ZEKE spectrum is linked to the shortening of the intermolecular bond formed between the two moieties. Multidimensional Franck–Condon simulations of the REMPI and MATI spectra of phenol–nitrogen generated using equilibrium geometries obtained from the CASSCF, MRCI, and SACCI *ab initio* methodologies are presented and analyzed in the following sections of this paper. To the best of our knowledge, the first multidimensional Franck–Condon simulations of ZEKE/MATI spectra are presented here. The underlying theory and the computational code developed for the multidimensional Franck–Condon simulations have been described in the preceding paper,¹³ where the program was employed for the Franck–Condon simulations of the DF spectra of phenol on the basis of CASSCF, MRCI, and SACCI *ab initio* calculations. The rotational simulations presented were carried out using an asymmetric rotor program developed by M. S. Ford.²¹

2. *Ab Initio* Calculations

2.1. Methodologies. Watkins et al.¹⁷ performed (8,7)-CASSCF/cc-pVDZ geometry optimizations and normal-mode analyses of the S_0 , S_1 , and D_0 states using the same active space employed

TABLE 1: S_0 , S_1 , and D_0 State Rotational Constants Obtained from the CASSCF, MRCI, and SACCI Equilibrium Geometries of Phenol–Nitrogen (the Dunning-Type Basis Set cc-pVDZ Was Used for All Calculations)

state	rotational		CASSCF ^a	MRCI	SACCI	expt ^b	expt ^c
	constant						
S_0	A		4067.3	4087.9	4105.4	4072.2	4046.6 + 4.2
	B		620.3	620.8	616.8	648.0	587.4 + 2.3
	C		538.2	538.9	536.2	559.3	538.4 + 0.5
S_1	A		3931.6	3963.3	4014.2	3930.7	4011.9 + 4.5
	B		615.9	616.8	627.1	663.7	631.7 + 2.7
	C		532.5	533.7	542.4	567.8	524.7 + 0.9
D_0	A		4266.8	4282.5	4271.4		
	B		679.1	679.6	671.3		
	C		585.9	586.5	580.1		

^a Results taken from ref 17. ^b Results from fit to high resolution LIF spectra; see ref 20. ^c Results from fit to vibrationless REMPI band contour; see ref 16.

for the phenol monomer.²² Their results were used for the rotational and Franck–Condon simulations that follow.

Internally contracted MRCI/cc-pVDZ geometry optimizations of the S_0 , S_1 , and D_0 states of phenol–nitrogen have been performed using the state-specific CASSCF wave functions described in ref 17. The MRCI wave functions of the S_0 and S_1 states consisted of 4 723 992 uncontracted configuration space functions (CSFs), which were internally contracted to 241 332 configurations. For the D_0 state, 5 276 334 uncontracted CSFs were internally contracted to 251 622 configurations.

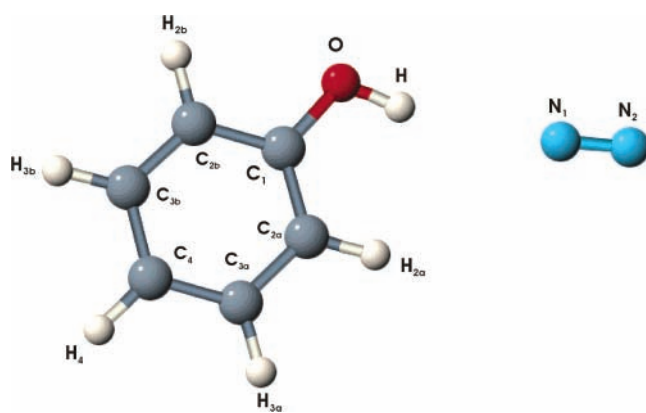
SACCI/cc-pVDZ geometry optimizations of the S_0 , S_1 , and D_0 states have been performed using the full valence space as active space. For calculation efficiency, the (8,7)-CASSCF/cc-pVDZ geometries were used as starting geometries for the optimization. All single excitation operators were included in the linked terms of the SACCI calculations. A level two perturbation selection was carried out for the linked double excitation operators. No R2S2-type unlinked operators were included. This led to an excitation space of 43 586 operators for the SAC wave function, 30 962 operators for the S_1 SACCI wave function, and 7233 operators for the D_0 SACCI wave function. The geometries obtained after three macroiterations were used for the Franck–Condon simulations.

MRCI calculations were performed with MOLPRO version 2002.⁶²³ and SACCI calculations with Gaussian 03²⁴ on an IBM RS/6000 (4x Power3 375 MHz 64-bit RISC, model 44P270, AIX 5.1L, 4 Gb RAM, 64 Gb scratch) and Linux PC (2x Pentium III 32-bit, Redhat Linux 9.0, 2 Gb RAM, 16 Gb scratch).

2.2. Geometries: Rotational Constants and Simulations.

Very accurate rotational constants of the S_0 and S_1 states of phenol have been measured by Ford et al.¹⁶ and Schmitt et al.²⁰ The former obtained constants and transition dipole moments by fitting to the partially rotationally resolved band contour of the S_1^0 vibrationless origin, and the latter, by fitting to high resolution (40 MHz) LIF spectra of the same vibronic transition. Table 1 lists these constants together with the constants obtained from the CASSCF, MRCI, and SACCI geometries. The ratios of the a and b transition dipole moments quoted in both studies are somewhat different: $\mu_{a/b} = 0.52$ in ref 16 and $\mu_{a/b} = 0.58$ in ref 20. Table 2 lists the S_0 – S_1 and S_1 – D_0 geometry changes.

To visualize the quality of the calculated geometries, rotational profiles of the vibrationless S_1^0 band origin were simulated with the rotational constants in Table 1 and compared to the partially rotationally resolved 1 + 1' REMPI spectrum of ref 16. The results are shown in Figure 1. The temperature,

TABLE 2: S_0-S_1 and S_1-D_0 Induced Bond Length Changes of Phenol–Nitrogen (for Atom Labels, Refer to the Graphic above the Table)^a


	S_0-S_1 changes			S_1-D_0 changes		
	C^b	M	S	C^b	M	S
Bond Length/pm						
N_1-N_2	0.0	0.0	-0.1	-0.1	-0.1	0.1
$H-N_1$	-1.2	-0.9	-6.2	-40.3	-40.6	-32.0
$O-H$	0.1	0.1	0.3	1.6	1.3	1.0
$C-OH$	-0.7	-1.0	-2.0	-7.7	-5.9	-4.4
C_1-C_{2a}	3.7	3.5	2.9	0.7	0.3	0.8
$C_{2a}-C_{3a}$	3.4	3.3	2.8	-6.5	-6.1	-5.5
$C_{3a}-C_4$	4.1	3.7	3.1	-1.0	-0.8	-0.5
$C_{3b}-C_4$	3.5	3.2	2.4	-1.5	-1.3	-0.3
$C_{2b}-C_{3b}$	4.2	4.0	3.1	-6.4	-6.1	-5.5
C_1-C_{2b}	2.9	2.9	2.6	1.1	0.9	1.6
$C_{2a}-H_{2a}$	-0.2	-0.3	-0.2	0.0	0.0	-0.1
$C_{3a}-H_{3a}$	-0.3	-0.3	-0.4	0.1	0.1	0.0
C_4-H_4	0.0	0.0	0.1	-0.1	0.0	-0.2
$C_{3b}-H_{3b}$	-0.3	-0.3	-0.4	0.1	0.1	0.0
$C_{2b}-H_{2b}$	-0.2	-0.2	-0.3	0.1	0.1	0.1
Angle/deg						
$O-H_1-N_1$	-0.6	-0.8	-0.1	0.5	1.0	1.8
$H-N_1-N_2$	0.4	0.5	0.4	-0.1	-0.5	-1.2
C_1-O-H	0.1	0.1	0.2	4.7	4.4	4.5
$C_{2a}-C_1-O$	-1.1	-1.4	-1.5	0.9	1.4	2.0
$C_{2a}-C_1-C_{2b}$	1.9	2.1	3.0	-0.9	-1.1	-1.7
$C_1-C_{2a}-C_{3a}$	-0.9	-1.1	-1.9	-0.2	0.0	0.4
$C_{2a}-C_{3a}-C_4$	-0.7	-0.9	-1.1	0.8	0.7	1.0
$C_{3a}-C_4-C_{3b}$	1.5	1.9	2.8	-0.3	-0.3	-0.8
$C_{2b}-C_{3b}-C_4$	-0.9	-1.1	-1.5	0.6	0.4	0.4
$C_1-C_{2b}-C_{3b}$	-0.8	-1.0	-1.3	0.0	0.3	0.7
$C_1-C_{2b}-H_{2b}$	0.2	0.2	0.0	-1.1	-1.0	-1.0
$C_1-C_{2a}-H_{2a}$	0.2	0.2	0.2	-0.9	-0.6	-0.3

^a C, CASSCF; M, MRCI; S, SACCI. ^b Values taken from ref 17.

resolution, and transition dipole moments in the simulations were 4.3 K, 1500 MHz, and $\mu_{a/b} = 0.52$, as quoted in ref 16.

Inspection of Table 1 reveals that SACCI rotational constants are closest to the experimental values obtained from the fit to the partially rotationally band contour of ref 16. The opposite is true for the CASSCF constants, which are closest to the values obtained from the high resolution LIF spectra. This is reflected in the partially rotationally resolved band profiles shown in Figure 1, where the SACCI trace delivers the best fit to experiment. In particular, the P branch is modeled quite truthfully. For the R branch, however, all three simulations suffer from the same shortcoming, whereby the intensity ratio of the intense peaks at +10 000 and +20 000 MHz is inverted compared to the experiment.

To get a better comparison between theory and experiment, high resolution simulations have been carried out and compared to the high resolution LIF spectrum of Schmitt et al.²⁰ In this second set of simulations, the resolution and temperature were

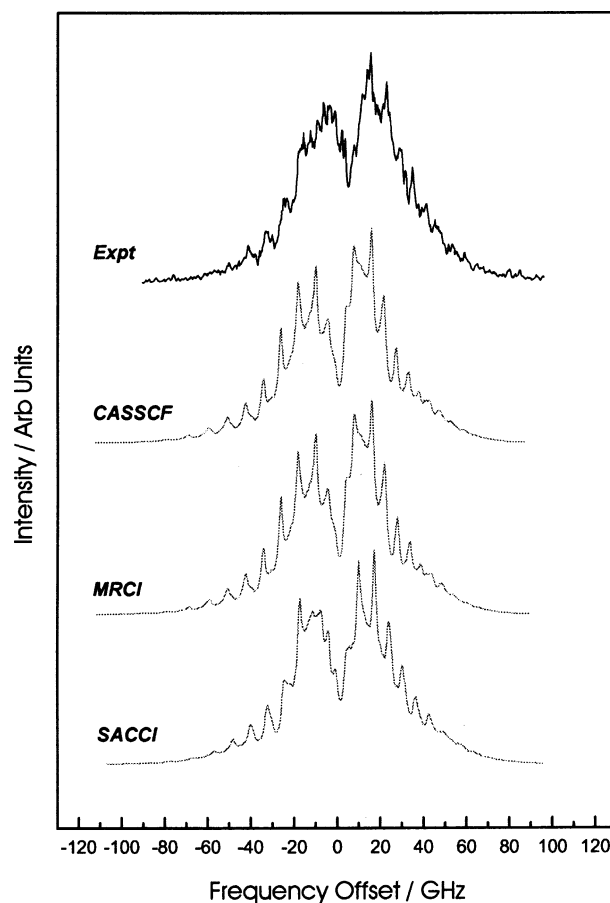


Figure 1. Rotational profiles of the S_10^0 vibrationless origin band of phenol. The experimental trace was obtained from the authors of ref 16. The resolution was set to 1500 MHz and the rotational temperature to 4.3 K.

set to 40 MHz and 4.03 K, as per ref 20. The high resolution experimental spectrum recorded by Schmitt was reproduced by simulation using the experimental rotational constants reported in ref 20 and listed in Table 1. The results are shown in Figure 2.

Despite the similarity in the CASSCF rotational constants to the high resolution LIF constants, the simulations obtained from the SACCI constants gave the best fit. Not only is the P branch nicely represented, but also, the high intensity peaks at +10 000 and +20 000 MHz in the R branch are reproduced with the correct intensity ratio. The only explanation for this surprising outcome lies in the change of the rotational constants upon electronic excitation. Both CASSCF and MRCI deliver much closer predictions to experiment for the change of the A rotational constants (-135.7 and -124.5 MHz, respectively). However, they predict both the B and C rotational constants to decrease, while the experiment shows the exact opposite. SACCI underestimates the change of the rotational constant A (-91.2 MHz) but gives very close predictions to experiment for the changes in the rotational constants B and C ($+10.3$ and $+6.2$ MHz, respectively).

On the whole, however, the line intensities and energies of the simulation with SACCI rotational constants are not as faithfully reproduced as in the simulations of phenol shown in ref 13. This is because the geometries obtained after three macroiterations are not operator guess independent converged geometries. Further macroiterations or a larger number of excitation operators spanning a wider range of the complete potential energy surface of the cluster are needed to improve

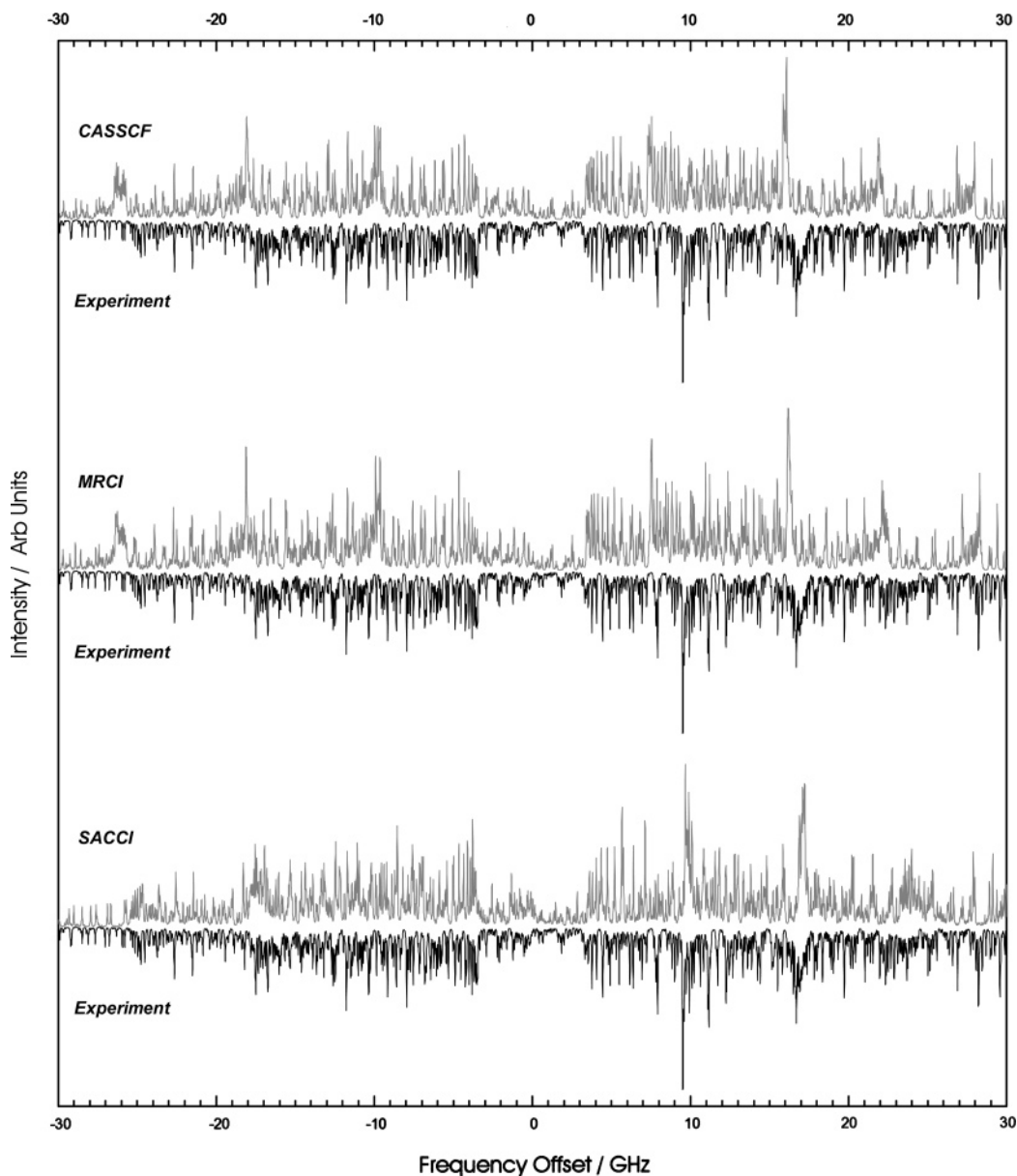


Figure 2. High resolution rotational spectra of the $S_1 0^0$ vibrationless origin using the rotational constants from ref 20 and (8,7)-CASSCF, MRCI, and SACCI S_0 and S_1 optimized geometries. The data are listed in Table 1. The resolution is 40 MHz, the temperature is 4.03 K, and the transition dipole moment ratio is $\mu_{ab} = 0.58$.

the SACCI geometries. The rotational simulations, however, show that the SACCI geometries obtained after three macroiterations, although not operator guess independent, already offer an improved description to the system compared to CASSCF and MRCI.

2.3. Normal-Mode Analysis. As with phenol, the normal-mode analysis for the three sets of geometries was carried out at the CASSCF level of theory. However, the CASSCF normal-mode analyses on the MRCI and SACCI optimized geometries yielded negative frequencies in the intermolecular modes because of the sensitivity of the CASSCF potential to even minor geometric alterations.

To overcome this problem, the CASSCF normal-mode analysis obtained from the CASSCF equilibrium geometries was used in all of the Franck–Condon simulations that follow. The CASSCF equilibrium geometries of the lower and upper state were simply replaced by the MRCI and SACCI equilibrium geometries. This effectively shifts the $3N - 6$ harmonic CASSCF potentials in the $3N$ space of the molecule to the MRCI or SACCI equilibrium point, thus changing the overlap integrals.

There is no doubt that this approach is questionable. However, it is not much different to the Franck–Condon fit procedure used in ref 12, where the geometry is altered systematically along some normal coordinate to optimize the overlap between experimental and simulated intensities, but the L -matrices and thus the normal modes themselves are left unchanged. A further justification for this strategy lies in the close agreement between experimental and CASSCF frequencies obtained from CASSCF equilibrium geometries (discussed extensively in ref 17), which indicates that the CASSCF harmonic potentials accurately describe the vibration potential surfaces in the small displacement regime. Table 3 lists the CASSCF frequencies for the S_0 , S_1 , and D_0 states obtained from ref 17. The same nomenclature that was used with phenol was also used for the intramolecular vibrations. The intermolecular vibrations are labeled according to the nomenclature used by Chapman et al.¹⁵

2.4. Duschinsky Rotations. The Duschinsky matrix obtained from the overlap between the S_0 and S_1 normal modes is shown in Figure 3a. There are four blocks of noninteracting vibrations.

TABLE 3: CASSCF Frequencies of Phenol–Nitrogen^a

mode number	assignment			CASSCF frequency ^b		
	S ₀	S ₁	D ₀	S ₀	S ₁	D ₀
Intermolecular Modes						
1	<i>1β'</i>	<i>1β''</i>	<i>1β'''</i>	10	6	35
2	<i>1β'</i>	<i>1β'</i>	<i>1β'</i>	19	20	36
3	<i>1σ</i>	<i>1σ</i>	<i>1σ</i>	57	58	105
4	<i>1γ''</i>	<i>1γ''</i>	<i>1γ''</i>	71	71	132
5	<i>1γ'</i>	<i>1γ'</i>	<i>1γ'</i>	77	79	133
Intramolecular Modes						
6	<i>10b</i>	<i>10b</i>	<i>10b</i>	251	184	195
7	<i>τ(OH)</i>	<i>16a</i>	<i>16a</i>	357	272	386
8	15	<i>τ(OH)</i>	15	435	346	467
9	<i>16a</i>	<i>16b</i>	<i>16b</i>	436	377	482
10	<i>16b</i>	15	6a	554	422	552
11	6a	4	6b	563	473	600
12	6b	<i>10a</i>	4	664	498	665
13	4	6a	<i>10a</i>	721	507	786
14	<i>11</i>	<i>11</i>	<i>11</i>	775	540	827
15	<i>10a</i>	6b	<i>τ(OH)</i>	837	582	862
16	1	<i>17a</i>	1	872	592	867
17	<i>17b</i>	<i>17b</i>	<i>17b</i>	898	616	932
18	<i>17a</i>	5	5	975	701	1016
19	5	1	<i>17a</i>	1000	824	1017
20	12	12	12	1068	970	1023
21	18a	18b	18a	1093	1014	1054
22	18b	18a	18b	1145	1032	1136
23	9b	9a	9b	1186	1216	1207
24	9a	9b	9a	1251	1234	1266
25	<i>β(OH)</i>	<i>β(OH)</i>	<i>β(OH)</i>	1275	1291	1294
26	14	13	14	1363	1374	1421
27	13	3	3	1384	1440	1474
28	3	19b	13	1465	1512	1520
29	19b	19a	19b	1597	1547	1593
30	19a	8b	19a	1635	1676	1646
31	8b	8a	8b	1740	1700	1649
32	8a	14	8a	1758	1863	1787
33	<i>σ(N₂)</i>	<i>σ(N₂)</i>	<i>σ(N₂)</i>	2763	2763	2768
34	20a	20a	20a	3323	3349	3368
35	7a	7a	7a	3335	3355	3378
36	7b	7b	7b	3347	3370	3385
37	20b	20b	20b	3361	3379	3393
38	2	2	2	3369	3392	3399
39	<i>σ(OH)</i>	<i>σ(OH)</i>	<i>σ(OH)</i>	4161	4156	3893

^a Out-of-plane vibrations are in italics. All values are given in wavenumbers. ^b Data taken from ref 17.

As with phenol (see refs 11 and 13), these are the out-of-plane and in-plane vibrations, as they belong to different symmetry elements in the C_s point group. The CH stretching vibrations 20a, 7a, 7b, 20b, and 2 constitute a block of their own, and additionally, a fourth block is formed by the intermolecular vibrations. Among the phenol–nitrogen intramolecular in-plane vibrations, the same Duschinsky rotations are observed as with the monomer. No rotations occur in the intermolecular modes. Large mode scrambling occurs in the out-of-plane modes, as expected.

The Duschinsky matrix obtained from the overlap between the normal modes of the S₁ and D₀ states has the same blocks as the S₀–S₁ matrix and is shown in Figure 3b. Similar rotations can also be observed. Modes 18a and 12 and modes 9a and 9b are Duschinsky active, but unlike the S₀–S₁ matrix, the latter do not rotate with mode 14 or β (OH). Considerable mode scrambling occurs with mode 14, as it changes quite considerably in the D₀ state

3. Franck–Condon Simulations

3.1. Franck–Condon (FC) Simulation of the REMPI Spectrum. Enlarged views of the intermolecular region of the Franck–Condon simulations obtained from CASSCF and

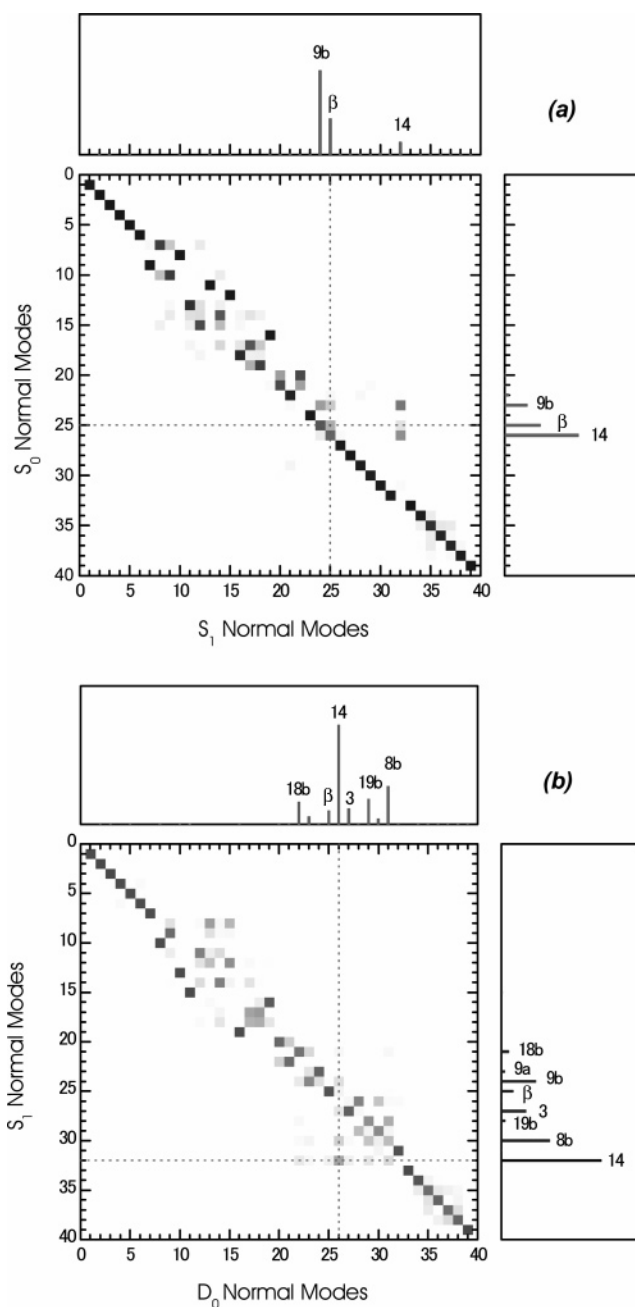


Figure 3. Plot of the squares of the elements of the Duschinsky matrix \mathbf{S} obtained by overlapping the CASSCF normal modes of (a) the S₀ and S₁ states and (b) the S₁ and D₀ states. The darker the square, the closer the respective matrix element is to unity. The axes list the normal modes in terms of mode numbers. To relate mode numbering to assignment, see Table 3. In part a, the profile graphs show the Duschinsky rotation of mode β (OH) for an S₁–S₀ transition (right profile window) and an S₀–S₁ transition (top profile window). In part b, the profile graphs show the Duschinsky rotation of mode 14 for a D₀–S₁ transition (right profile window) and an S₁–D₀ transition (top profile window).

SACCI geometries are shown in Figure 4 together with the experimental spectrum spanning the same energy region. The MRCI simulation is not shown, as it is essentially identical to that obtained from the CASSCF geometries.

Simulations of the phenol–nitrogen REMPI spectrum with an extended energy window up to 2500 cm⁻¹ have been carried out but are not shown. A comparison to the DF spectrum of the electronic origin of the phenol monomer of ref 13 reveals a great similarity between the simulations in terms of intensities and related intramolecular vibrations, suggesting that the

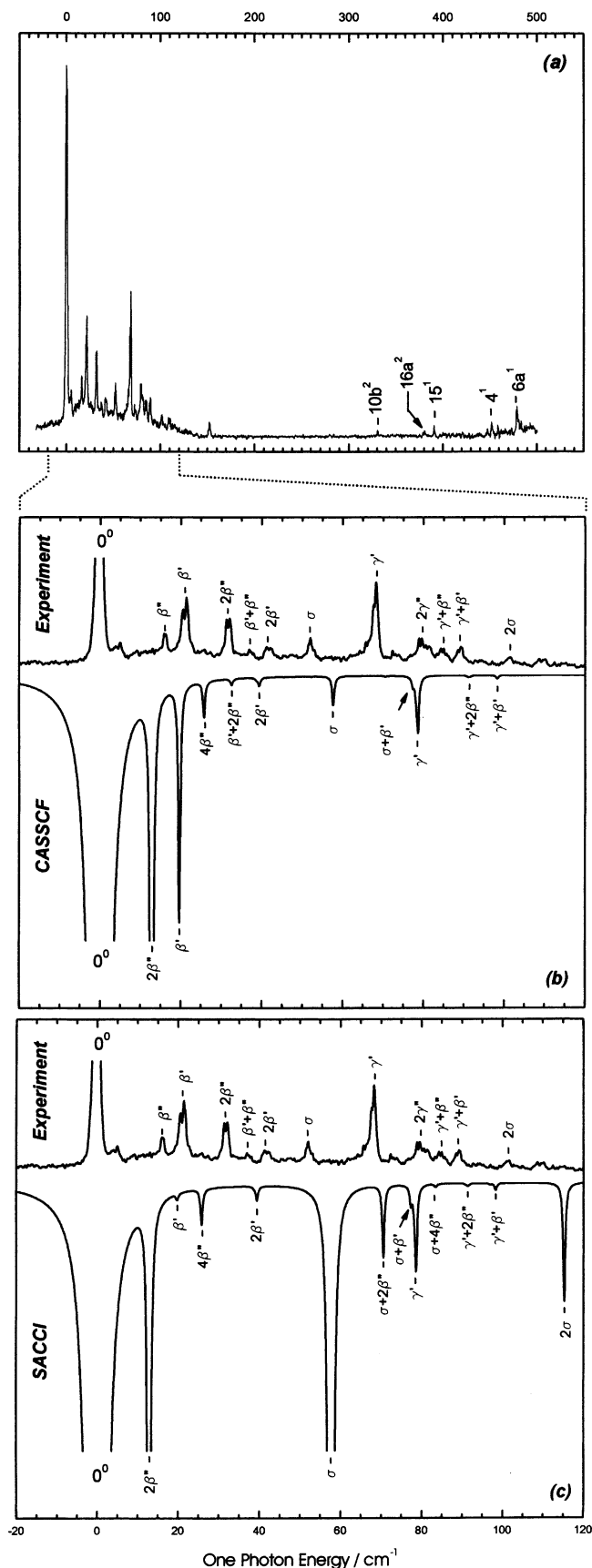


Figure 4. Intermolecular mode region of the experimental (a) and simulated REMPI spectrum obtained from (b) CASSCF and (c) SACCI equilibrium geometries.

predicted S_0 – S_1 geometry changes of phenol itself are not greatly affected by the N_2 moiety at the levels of theory used.

As with phenol, the simulations obtained from CASSCF and MRCI geometries are almost identical and suffer from the same shortcomings in that they fail to correctly represent the intensities in mode 6a. The simulation with SACCI geometries shows similar differences with respect to CASSCF and MRCI as with the phenol monomer. Mode 6a and its combination bands are more intense, while modes 12 and related combinations lose intensity.

The first 120 cm^{-1} of the experimental $1 + 1'$ REMPI spectrum of phenol–nitrogen show vibrational bands associated with intermolecular modes¹⁵ (see Figure 4). Unlike the experimental spectrum, in the simulations, the transitions associated with the intramolecular modes of the phenol moiety are far more intense than the transitions associated with the intermolecular modes. There is, however, some improvement in the SACCI simulation, which shows a transition associated with the intermolecular stretching mode σ of equal intensity to the transition associated with mode 6a.

The bands in the REMPI spectrum are assigned according to refs 14–16, while the bands in the simulations are labeled according to the Franck–Condon predictions. It is clear from the difference between experiment and simulations that an experimental assignment is very difficult to make with confidence on the basis of the Franck–Condon simulations, most likely due to the failure of the simulations to take anharmonic effects into account. This can be clearly seen from the fact that bands associated with mode β'' and combination bands $\beta' + \beta''$ and $\gamma' + \beta''$ are observed in the spectrum. As mode β'' has a'' symmetry, transitions to these vibrations are not symmetry allowed and therefore are not reproduced in the simulations. Furthermore, the bands in the REMPI spectrum assigned to mode β'' are closer in energy to $2\beta''$ or β' in the simulations, while band $\beta' + \beta''$ coincides with the combination band $\beta' + 2\beta''$.

In the simulations obtained from CASSCF equilibrium geometries, bands $2\beta'$, σ , and γ' are in good agreement with the REMPI spectrum both in energy and relative intensity, although their absolute intensities are too low. The underestimation of the transition intensities arising from intermolecular modes corroborates a fact already pointed out by Schmitt et al.,²⁰ that CASSCF underestimates the S_0 – S_1 induced change of the intermolecular binding. As can be seen from the values in Table 2, CASSCF predicts the H– N_1 bond to contract by 1.2 pm upon excitation, while fits to the high resolution rotational LIF spectra in ref 20 show the bond shortening to be between 10 and 15 pm.

The SACCI calculations predict a larger change in the H– N_1 bond length, although the contraction of 6.2 pm is still smaller than the experimental value. Nonetheless, this change results in more intense transitions in the intermolecular modes. In particular, modes σ and 2σ gain considerable intensity in SACCI based Franck–Condon simulations. The transitions associated with the intermolecular in-plane and out-of-plane bends, β' and β'' , as well as the in-plane wag γ' , suggest that the SACCI predicted S_0 – S_1 change of the angles O–H– N_1 and H– N_1 – N_2 is underestimated.

3.2. FC Simulation of the MATI Spectrum Recorded via the S_{10}^0 Intermediate. Vibronic symmetry selection rules in one-photon MATI spectra have been extensively discussed in refs 25 and 26. They can easily be extended to two-photon MATI transitions involving an intermediate electronic state. In the Born–Oppenheimer approximation, the wave function of both the electronic intermediate Ψ^I and the Rydberg state Ψ^R is separated into an electronic (e) and vibrational (v) wave

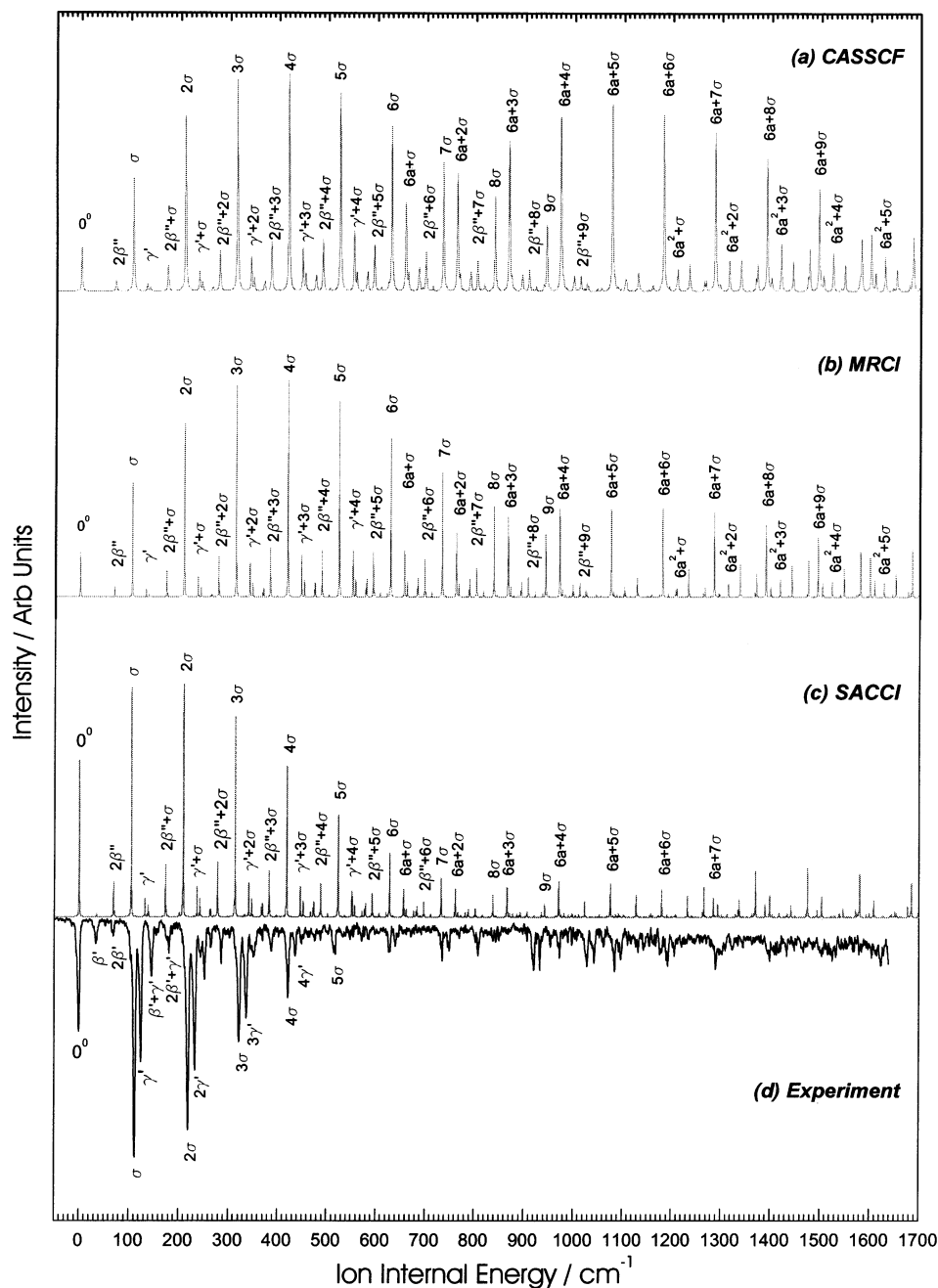


Figure 5. Franck–Condon simulations of the MATI spectrum via the S_10^0 origin obtained from (a) CASSCF, (b) MRCl, and (c) SACCI S_1 and D_0 equilibrium geometries together with the corresponding experimental MATI spectrum (d). The peaks of the MATI spectrum are labeled according to the assignments in refs 14–16, while the peaks in the simulations are labeled following the Franck–Condon predictions.

function. The electronic wave function of the Rydberg state is furthermore expressed as a product of the ionic core Ψ_e^C and the Rydberg electron Ψ_e^R . Thus, the transition dipole moment integral separates out into a product of integrals between the electronic and vibrational wave functions: $\langle \Psi^I | \hat{\mu} | \Psi^R \rangle = \langle \Psi_e^I | \hat{\mu} | \Psi_e^C \Psi_e^R \rangle \langle \Psi_v^I | \Psi_v^C \rangle$. For a high- n Rydberg state, Ψ_e^C and Ψ_v^C can be approximated as those of the corresponding ionic state. One can always choose a Rydberg orbital that makes the electronic part of the transition dipole moment allowed. Alternatively, one can argue that the symmetry of the ionic state is a product of the symmetry of the cationic core and the departing photoelectron. In the case of phenol–nitrogen, which has C_s point group symmetry, cationic core and photoelectron have a'' symmetry. Thus, the overall symmetry of the ionic state is a' . As the transition dipole moment operator $\hat{\mu}$ lies in the

plane of the aromatic ring and has therefore a' symmetry, the electronic part of the transition dipole moment integral is totally symmetric. Thus, the vibronic intensities of two-color MATI spectra are determined by the Franck–Condon factors $\langle \Psi_v^I | \Psi_v^C \rangle$ and the same selection rules hold as those for S_0 – S_1 vibronic transitions. The two-color MATI spectra presented here have been recorded via totally symmetric vibrational states of the S_1 intermediate. Hence, Ψ_v^I has a' symmetry. To obtain nonzero Franck–Condon factors, Ψ_v^C must also belong to a' . This implies that fundamentals and all overtones of a' modes are allowed, while the $\Delta v = 2, 4, 6$ selection rule holds for a'' modes. Similarly, transitions to vibronic combination states with a' symmetry are allowed.

Franck–Condon simulations of the MATI spectrum recorded via the S_10^0 origin based on CASSCF, MRCl, and SACCI

equilibrium geometries are shown in Figure 5, together with the corresponding experimental spectrum. As with the REMPI spectrum, the bands in the MATI spectrum are labeled according to the assignments in refs 14–16, while those in the simulations are labeled following the Franck–Condon predictions.

Some major differences can be observed between experiment and the simulation obtained from CASSCF equilibrium geometries (see Figure 5a). The simulated envelope of the $n\sigma$ progression is much more extended with strong transitions up to nine quanta, while the progression in the experiment dies off after five quanta. Furthermore, progressions arising from the $6a + n\sigma$ and $1 + n\sigma$ combination bands appear in the simulated spectrum with equal intensity to the $n\sigma$ progression. The intense and extended envelopes suggest that the predicted H–N₁ bond length change is overestimated. This is corroborated by the one-dimensional Franck–Condon simulations carried out by Haines et al.,¹⁴ who estimated the H–N₁ bond to contract upon the S₁–D₀ transition by 26.2 pm. This is substantially smaller than the CASSCF value of 40.2 pm.

MRCI predicts a slightly larger change (40.3 pm) in the H–N₁ bond length which results in a similar extended envelope of the $n\sigma$ progression. However, the $6a + n\sigma$ and $1 + n\sigma$ combination bands are considerably less intense compared to the simulation obtained from CASSCF. From the DF simulations on phenol in ref 13, it is clear that the intensity of modes $6a$ and 1 and relative combination bands is controlled by the CO bond length change. The larger the change, the higher the transition intensity associated with these modes. MRCI predicts a smaller contraction in the C–O bond (5.9 pm) compared to CASSCF (7.7 pm). This results in less intense $6a + n\sigma$ and $1 + n\sigma$ progressions.

A considerably improved simulation is obtained when SACCI geometries are employed. The predicted H–N₁ bond length change of 32 pm is much closer to the empirical value of Haines et al.¹⁴ This causes the $n\sigma$ progression to die off more rapidly, and the simulated envelope closely resembles the experimental one. The contraction of the C–O bond is lower than that for MRCI which makes the bands in the $6a + n\sigma$ and $1 + n\sigma$ progressions less intense compared to the MRCI based simulation, thus bringing the simulation as a whole closer to the appearance of the experimental spectrum.

However, there are some differences between simulation and experiment that still remain even in the much improved spectrum obtained from the SACCI geometries. These differences mainly concern the γ' progression. In all simulations, the γ' fundamental is the only member of the progression which appears with significant intensity, while higher members are essentially not observed. However, in the experimental spectrum, the bands assigned to the $n\gamma'$ progression by Haines et al.¹⁴ are almost as intense as the corresponding bands in the $n\sigma$ progression. All simulations suggest that this progression is not due to bands arising from the in-plane wag γ' but rather is due to combination bands involving one quantum of the wag and n quanta of the stretch, that is, a $\gamma' + n\sigma$ progression. This suggestion is, however, to be taken with care. Haines et al.¹⁴ argued that the in-plane wag γ' potential is very anharmonic by analogy with findings of similar modes in other hydrogen bonded phenol clusters.^{27–29} If this is the case, then the predictions of the Franck–Condon simulations are incorrect, as they are based on the harmonic approximation. However, comparison to the MATI spectrum of phenol–carbon monoxide in ref 30 suggests that the prediction obtained from the Franck–Condon simulations might be correct. Like phenol–nitrogen, phenol–carbon monoxide displays two prominent progressions in its MATI

spectrum recorded via the S₁⁰ origin. One progression was assigned to the intermolecular stretch σ , and the other, based on ab initio MP2/cc-pVDZ frequencies and with a comparable Franck–Condon intensity envelope, to $\gamma' + n\sigma$. Due to the similarity between the MATI spectra, structure, and type of intermolecular interaction of the two clusters, the prediction of the Franck–Condon simulations that the progression adjacent to the σ progression in the phenol–nitrogen MATI spectrum is associated with the $\gamma' + n\sigma$ combination band can therefore not be ruled out, though this second possibility does assume that the γ' wag and the σ stretch progression are rather less anharmonic in lower quanta than what was originally suggested.¹⁴ While some further ab initio work does lend some degree of support for the initial experimental assignment,¹⁵ we feel that the available data at this stage are too equivocal to suggest either confirmation of the current assignment or reassignment without further evidence.

3.3. FC Simulation of the MATI Spectrum Recorded via the S₁ γ' Intermediate. Franck–Condon simulations of the MATI spectrum recorded via the S₁ γ' intermediate state obtained from CASSCF and SACCI S₁ and D₀ equilibrium geometries are shown in Figures 6 and 7, respectively, together with the corresponding experimental spectrum. The bands in the MATI spectrum are labeled according to the assignments in refs 14–16, while those in the simulations are labeled following the Franck–Condon predictions. The simulation obtained from MRCI geometries is not shown, since in the energy window of the experimental spectrum it is identical to the CASSCF simulation in Figure 6.

As in the previous section, the $n\sigma$ progression in the simulation obtained from CASSCF equilibrium geometries is much more extended than that in the experimental spectrum. This improves in the simulations with SACCI geometries. As with the MATI S₁⁰ simulations, the most prominent progression after $n\sigma$ is the $\gamma' + n\sigma$ progression, which also has a less extended envelope in the simulation obtained from SACCI geometries. It is, however, surprising to see that it is this progression, and not a progression in γ' , that shows enhanced intensities. This reinforces the suggestion in the simulations of the previous section that the progression assigned to $n\gamma'$ in the experimental spectrum is more likely to be due to transitions to $\gamma' + n\sigma$ vibrations. Anharmonicity effects ascribed to the in-plane wag prevent a reassignment of the $n\gamma'$ progression to $\gamma' + n\sigma$. However, a similar argument to the one discussed in the previous section regarding the MATI spectra of the analogous species phenol–carbon monoxide³⁰ does not allow the assignment suggested by the Franck–Condon simulations to be ruled out.

Interestingly, the $n\sigma$ and $\gamma' + n\sigma$ progressions appear to be mutually exclusive in the simulations. This can be seen from the fact that, in the MATI S₁⁰ simulations, the $n\sigma$ progression is strong and the $\gamma' + n\sigma$ progression is weak, while the opposite is true for the MATI S₁ γ' simulations. However, in both the MATI S₁⁰ and MATI S₁ γ' experimental spectra, the $n\sigma$ and $n\gamma'$ progressions are of comparable intensities, suggesting that the $n\gamma'$ progression should not be reassigned to $\gamma' + n\sigma$.

The prominent decline in intensity of the bands 2σ and $2\gamma'$ which disrupts the progression envelope in the experimental MATI spectrum and is ascribed to a direct self-canceling overlap between the $v = 1\gamma'$ vibrational wave function of the S₁ state and the $v = 2\gamma'$ and σ wave functions of the D₀ state is not reproduced in any of the simulations. This conclusively indicates that even for the much improved SACCI geometries the H–N₁ bond contraction is still overestimated and the change in the

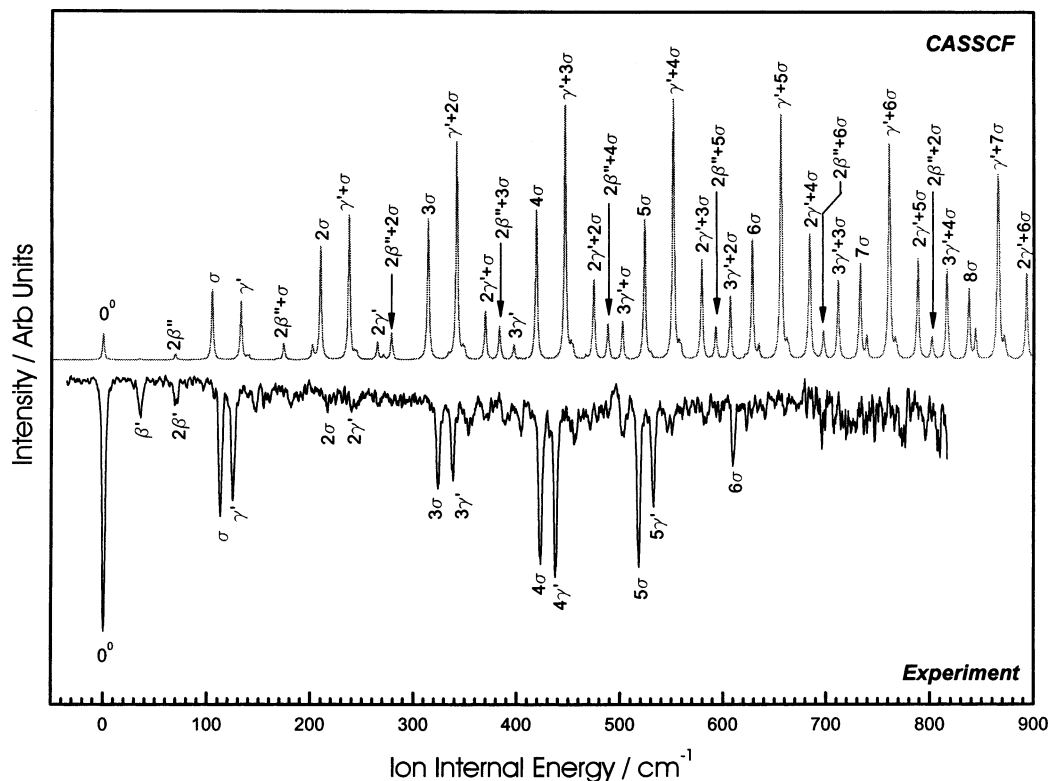


Figure 6. Franck–Condon simulations of the MATI spectrum via the $S_1\gamma'$ in-plane wag obtained from CASSCF S_1 and D_0 equilibrium geometries together with the corresponding experimental MATI spectrum. The peaks of the MATI spectrum are labeled according to the assignments in refs 14–16, while the peaks in the simulations are labeled following the Franck–Condon predictions.

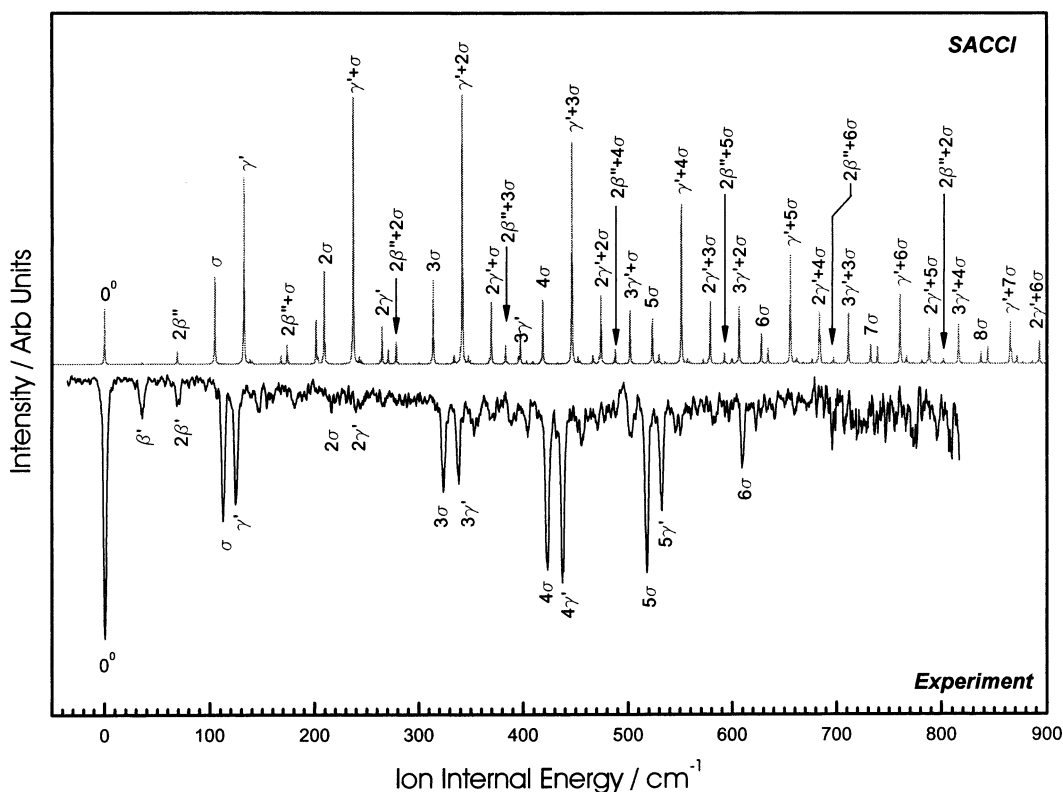


Figure 7. Franck–Condon simulations of the MATI spectrum via the $S_1\gamma'$ in-plane wag obtained from SACCI S_1 and D_0 equilibrium geometries together with the corresponding experimental MATI spectrum. The peaks of the MATI spectrum are labeled according to the assignments in refs 14–16, while the peaks in the simulations are labeled following the Franck–Condon predictions.

angles O–H– N_1 and H– N_1 – N_2 is still underestimated and illustrates the acute dependence of the intermolecular Franck–

Condon intensities on the orientation of the phenol and nitrogen moieties.

4. Concluding Remarks

Franck–Condon simulations of the phenol–nitrogen REMPI spectrum based on CASSCF equilibrium geometries underestimate the transition intensities arising from intermolecular modes because the predicted H–N₁ bond length change is too small. The opposite occurs in the MATI simulations: An overestimated H–N₁ bond length contraction for the S₁–D₀ electronic transition causes large and intense progressions of the intermolecular stretching mode together with combinations with intramolecular modes. Similar shortcomings are observed in the simulations obtained from MRCI geometries. Much improved simulations arise from the superior SACCI geometries, which predict H–N₁ bond length contractions that are much closer to the empirical values found by Schmitt²⁰ and Haines.¹⁴

Nonetheless, even the SACCI geometries in some cases fail to give good simulations. This is mainly attributed to the fact that the H–N₁ bond contraction is still underestimated for the S₀–S₁ transition and overestimated for the S₁–D₀ transition. Furthermore, the change in the angles O–H–N₁ and H–N₁–N₂ is always underestimated. This clearly indicates that improved geometries have to be obtained by carrying out calculations with larger numbers of excitation operators spanning a wider section of the intermolecular potential energy surface. It is also possible that the basis set description of the intermolecular potential energy surface is incomplete and further simulations may benefit from larger basis sets. However, it is clear from the Franck–Condon simulations presented that SACCI/cc-pVDZ is of suitable quality to give good replication of experimental spectra of phenol–nitrogen.

The MATI simulations suggest that the envelope due to the $n\gamma'$ progression should be reassigned to the $\gamma' + n\sigma$ progression, as is the case in the MATI spectra of phenol–carbon monoxide. However, this cannot be conclusively confirmed, as in-plane wags tend to be strongly anharmonic. Thus, to obtain a simulation that can aid the peak assignment of the phenol–N₂ MATI spectra, not only are high quality ab initio geometries required but also anharmonic effects in the calculation of the Franck–Condon integrals need to be included. It would be desirable to develop a generalized approach which combines both the harmonic and anharmonic description into a single model, as this will clarify how much anharmonicity affects the phenol–nitrogen MATI spectra and to what extent the harmonic approximation is appropriate in the investigation of the cluster spectra. The good agreement between harmonic ab initio frequencies and experiment (in the case of phenol–nitrogen and many other clusters similar to it) seems to suggest that it is a valid enough simplification.

Acknowledgment. We thank the EPSRC for funding this work (Grant No. GR/M48451/01). Special thanks go to Dr. M. C. R. Cockett for making useful comments and suggestions in the editing process of this manuscript.

References and Notes

(1) Sando, G. M.; Spears, K. G.; Kupp, J. T.; Ruhoff, P. T. *J. Phys. Chem. A* **2001**, *105*, 5317.

- (2) Hwang, H.; Rossky, P. J. *J. Phys. Chem. A* **2004**, *108*, 2607.
 (3) Hwang, H.; Rossky, P. J. *J. Phys. Chem. B* **2004**, *108*, 6723.
 (4) Borrelli, R.; Peluso, A. *J. Chem. Phys.* **2003**, *119*, 8437.
 (5) Duschinsky, F. *Acta Physicochim. URSS* **1937**, *7*, 441.
 (6) Sharp, T. E.; Rosenstock, H. M. *J. Chem. Phys.* **1964**, *41*, 3443.
 (7) Doktorov, E. V.; Malkin, I. A.; Manko, V. I. *J. Mol. Spectrosc.* **1977**, *64*, 302.
 (8) Gruner, D.; Brumer, P. *Chem. Phys. Lett.* **1987**, *138*, 310.
 (9) Callis, P. R.; Vivian, J. T.; Slater, L. S. *Chem. Phys. Lett.* **1994**, *244*, 43.
 (10) Berger, R.; Fischer, C.; Klessinger, M. *J. Phys. Chem. A* **1998**, *102*, 7147.
 (11) Schumm, S.; Gerhards, M.; Kleinermanns, K. *J. Phys. Chem. A* **2000**, *104*, 10648.
 (12) Spangenberg, D.; Imhof, P.; Kleinermanns, K. *Phys. Chem. Chem. Phys.* **2003**, *4*, 2404.
 (13) Pugliesi, I.; Müller-Dethels, K. *J. Phys. Chem. A*, submitted for publication.
 (14) Haines, S. R.; Geppert, W. D.; Chapman, D. M.; Watkins, M. J.; Dessent, C. E. H.; Cockett, M. C. R.; Müller-Dethels, K. *J. Chem. Phys.* **1998**, *109*, 9244.
 (15) Chapman, D. M.; Haines, S. R.; Geppert, W. D.; Müller-Dethlefs, K.; Peel, J. B. *J. Chem. Phys.* **1999**, *111*, 1955.
 (16) Ford, M. S.; Haines, S. R.; Pugliesi, I.; Dessent, C. E. H.; Müller-Dethlefs, K. *J. Electron. Spectrosc. Relat. Phenom.* **2000**, *112*, 231.
 (17) Watkins, M. J.; Müller-Dethlefs, K.; Cockett, M. C. R. *Phys. Chem. Chem. Phys.* **2000**, *2*, 5528.
 (18) Fujii, A.; Miyazaki, M.; Ebata, T.; Mikami, N. *J. Chem. Phys.* **1999**, *110*, 11125.
 (19) Solca, N.; Dopfer, O. *Chem. Phys. Lett.* **2000**, *325*, 354.
 (20) Schmitt, M.; Ratzer, C.; Meerts, W. L. *J. Chem. Phys.* **2004**, *120*, 2752.
 (21) Asymmetric Rotor Simulation (A.R.S.) program written by M. S. Ford, The University of York, 2000.
 (22) Schumm, S.; Gerhards, M.; Roth, W.; Gier, H.; Kleinermanns, K. *Chem. Phys. Lett.* **1996**, *263*, 126.
 (23) Amos, R. D.; Bernhardtsson, A.; Berning, A.; Celani, P.; Cooper, D. L.; Deegan, M. J. O.; Dobbyn, A. J.; Eckert, F.; Hampel, C.; Hetzer, G.; Knowles, P. J.; Korona, T.; Lindh, R.; Lloyd, A. W.; McNicholas, S. J.; Manby, F. R.; Meyer, W.; Mura, M. E.; Nicklass, A.; Palmieri, P.; Pitzer, R.; Rauhut, G.; Schütz, M.; Schumann, U.; Stoll, H.; Stone, A. J.; Tarroni, R.; Thorsteinsson, T.; Werner, H.-J. *MOLPRO, a package of ab initio programs, version 2002.6*.
 (24) Frisch, M. J.; Trucks, G. W.; Schlegel, H. B.; Scuseria, G. E.; Robb, M. A.; Cheeseman, J. R.; Montgomery, J. A., Jr.; Vreven, T.; Kudin, K. N.; Burant, J. C.; Millam, J. M.; Iyengar, S. S.; Tomasi, J.; Barone, V.; Mennucci, B.; Cossi, M.; Scalmani, G.; Rega, N.; Petersson, G. A.; Nakatsuji, H.; Hada, M.; Ehara, M.; Toyota, K.; Fukuda, R.; Hasegawa, J.; Ishida, M.; Nakajima, T.; Honda, Y.; Kitao, O.; Nakai, H.; Klene, M.; Li, X.; Knox, J. E.; Hratchian, H. P.; Cross, J. B.; Bakken, V.; Adamo, C.; Jaramillo, J.; Gomperts, R.; Stratmann, R. E.; Yazyev, O.; Austin, A. J.; Cammi, R.; Pomelli, C.; Ochterski, J. W.; Ayala, P. Y.; Morokuma, K.; Voth, G. A.; Salvador, P.; Dannenberg, J. J.; Zakrzewski, V. G.; Dapprich, S.; Daniels, A. D.; Strain, M. C.; Farkas, O.; Malick, D. K.; Rabuck, A. D.; Raghavachari, K.; Foresman, J. B.; Ortiz, J. V.; Cui, Q.; Baboul, A. G.; Clifford, S.; Cioslowski, J.; Stefanov, B. B.; Liu, G.; Liashenko, A.; Piskorz, P.; Komaromi, I.; Martin, R. L.; Fox, D. J.; Keith, T.; Al-Laham, M. A.; Peng, C. Y.; Nanayakkara, A.; Challacombe, M.; Gill, P. M. W.; Johnson, B.; Chen, W.; Wong, M. W.; Gonzalez, C.; Pople, J. A. *Gaussian 03*, revision C.01; Gaussian, Inc.: Wallingford, CT, 2004.
 (25) Lee, M.; Kim, M. S. *J. Chem. Phys.* **2003**, *119*, 5085.
 (26) Kwon, C. H.; Kim, H. L.; Kim, M. S. *J. Phys. Chem. A* **2003**, *107*, 10969.
 (27) Müller-Dethlefs, K.; Dopfer, O.; Wright, T. G. *Chem. Rev.* **1994**, *94*, 1845.
 (28) Dopfer, O.; Reiser, G.; Müller-Dethlefs, K.; Schlag, E. W.; Colson, S. D. *J. Chem. Phys.* **1994**, *101*, 974.
 (29) Cordes, E.; Dopfer, O.; Wright, T. G.; Müller-Dethlefs, K. *J. Chem. Phys.* **1993**, *97*, 7471.
 (30) Haines, S. R.; Dessent, C. E. H.; Müller-Dethlefs, K. *J. Chem. Phys.* **1999**, *111*, 1947.